Available online at www.sciencedirect.com
SCIENCE DIRECT®
Journal of Molecular Spectroscopy 219 (2003) 119–128
Journal of MOLECULAR SPECTROSCOPY
www.elsevier.com/locate/jms

# Fourier transform emission spectroscopy of CoCl in the 500 nm region

T. Hirao,[a,*] B. Pinchemel,[b] and P.F. Bernath[a]

[a] *Department of Chemistry, University of Waterloo, Waterloo, Ont., Canada N2L 3G1*
[b] *Laboratoire de Physique des Lasers, Atomes et Molécules, UMR CNRS 8523, Centre d'Etudes et de Recherches Lasers et Applications, Université de Lille I 59655, Villeneuve d'Ascq Cedex, France*

Received 23 October 2002

**Abstract**

Fourier transform emission spectra of CoCl were obtained with a tube furnace-DC discharge source in the 450-500 nm spectral region. In addition to observing two different band systems, which were assigned as $[20.7]^3\Phi_4$–$X^3\Phi_4$ and $[21.3]^3\Phi_4$–$X^3\Phi_4$ by Adam et al. [J. Mol. Spectrosc. 212 (2002) 111], we obtained data for additional sub-bands and vibrational levels. In contrast to the previous work, intense $Q$ branches are seen in the [21.3]-$X^3\Phi_4$ bands which indicate that these bands are likely $\Delta\Lambda \neq 0$ transitions. The equilibrium rotational constant $B_e$ for the ground $X^3\Phi_4$ state is 0.1801104(28) $cm^{-1}$, the equilibrium bond length is 2.065122(16) Å and $\Delta G_{1/2}$ is 430.418(5) $cm^{-1}$.


## 1. Introduction

Transition metal-containing molecules are known to have dense and complicated electronic band systems, in part because they have relatively small rotational constants. The bands frequently display severe perturbations, due to the numerous electronic states arising from the open *d*-shell on the metal atom. A detailed understanding of such spectra requires high spectral resolution. Even though the electronic spectra of some transition metal-containing molecules were obtained early in the last century, it has been a difficult task to interpret the spectra. A modern technique such as Fourier transform spectroscopy can reveal the structural properties of transition metal-containing species and generally improves our understanding of transition metal chemistry.

Although electronic transitions of CoCl were already observed in the 1930s [1–2], and numerous bands were found in the 420–795 nm region [3–9], no detailed interpretation of these spectra was available. Very recently, Adam et al. [10] carried out a high resolution laser excitation experiment on CoCl around 483.3 and 470.3 nm, following a low resolution survey between 415 and 700 nm. They applied the technique of laser ablation followed by jet expansion to generate cold CoCl. The spectra were assigned to two different $^3\Phi_4$–$X^3\Phi_4$ transitions ($[20.7]^3\Phi_4$–$X^3\Phi_4$ and $[21.3]^3\Phi_4$– $X^3\Phi_4$). They argued that the ground state of CoCl should be $X^3\Phi_i$ by analogy with the ground states of CoH and CoF, which are established as $X^3\Phi_i$ by both theoretical and experimental methods [11–17]. The relative intensities of $P$ and $R$ branches of the observed two transitions were similar, suggesting that these bands have $\Delta\Lambda = 0$ despite the presence of $Q$ branches. In the high resolution experiment the hyperfine structure arising from $^{57}$Co ($I = 7/2$) nuclei of CoCl was clearly resolved, suggesting that the electric configuration of the ground state is $(\text{core})(10\sigma)^2(4\pi)^4\ (1\delta)^3(5\pi)^3(11\sigma)^2$ and that two transitions involve a promotion of a $11\sigma$ electron into the $12\sigma$ orbital. High vibrational levels of the two upper states (up to $v = 5$ and 4 for $[20.7]^3\Phi_4$ and $[21.3]^3\Phi_4$, respectively) were seen in the low-resolution spectra, while only the lowest two vibrational levels were obtained for

* Corresponding author. Present address: Institute for Astrophysics and Planetary Sciences, Ibaraki University, 2-1-1 Bunkyo, Mito, Ibaraki 310-8512, Japan. Fax: +81-29-228-8361.
*E-mail address:* yoshi@mcs.ibaraki.ac.jp (T. Hirao).

0022-2852/03/$ - see front matter © 2003 Elsevier Science (USA). All rights reserved.
doi:10.1016/S0022-2852(03)00020-1

Table 1a
Observed line positions of $Co^{35}Cl$ in $cm^{-1}$

| | $[21.3]^3\Delta_3$ (or $^3\Phi_4$)–$X^3\Phi_4$[a] | | | | | $[21.0]^3\Delta_2$ (or $^3\Phi_3$)–$X^3\Phi_3$ | | |
|---|---|---|---|---|---|---|---|---|
| $v'$–$v''$ | 0–0 | | | 0–1 | | 0–0 | | |
| $J''$ | $P$ | $Q$ | $R$ | $Q$ | $R$ | $P$ | $Q$ | $R$ |
| 17 | | | | | | | 20970.424 | |
| 18 | | | | | | | 20970.117 | |
| 19 | | | | | | | | |
| 20 | | | | | | | 20969.449 | |
| 21 | | | | | | | 20969.103 | |
| 22 | | | | | | | 20968.731 | |
| 23 | | | | | | | 20968.335 | |
| 24 | | | | | | | 20967.933 | 20976.499 |
| 25 | | | | | | | 20967.516 | 20976.360 |
| 26 | | | | | 20830.676 | | 20976.271 | |
| 27 | | | | | 20830.605 | | 20966.618 | 20976.159 |
| 28 | | 21250.221 | | | | | 20966.136 | 20976.023 |
| 29 | | 21249.721 | 21260.005 | | | | 20965.643 | 20975.881 |
| 30 | 21238.958 | 21249.226 | 21259.787 | 20819.667 | 20830.241 | | 20965.144 | 20975.722 |
| 31 | 21238.107 | 21248.645 | 21259.594 | 20819.189 | 20830.123 | | 20964.624 | 20975.527 |
| 32 | 21237.209 | 21248.071 | 21259.363 | 20818.675 | 20829.977 | | 20964.053 | 20975.317 |
| 33 | 21236.245 | 21247.525 | 21259.145 | 20818.162 | 20829.802 | | 20963.513 | 20975.098 |
| 34 | 21235.335 | 21246.928 | 21258.892 | 20817.664 | 20829.592 | | 20962.939 | 20974.862 |
| 35 | 21234.397 | 21246.324 | 21258.593 | 20817.072 | 20829.385 | 20950.385 | 20962.337 | 20974.608 |
| 36 | 21233.427 | 21245.689 | 21258.291 | 20816.531 | 20829.161 | 20949.439 | 20961.728 | 20974.330 |
| 37 | 21232.424 | 21245.034 | 21257.989 | 20815.952 | 20828.920 | 20948.491 | 20961.099 | 20974.058 |
| 38 | 21231.407 | 21244.360 | 21257.656 | 20815.366 | 20828.682 | 20947.486 | 20960.466 | 20973.745 |
| 39 | 21230.345 | 21243.692 | 21257.315 | 20814.736 | 20828.362 | 20946.478 | 20959.766 | 20973.426 |
| 40 | 21229.350 | 21243.004 | 21256.937 | 20814.093 | 20828.128 | 20945.471 | 20959.113 | 20973.086 |
| 41 | 21228.303 | 21242.273 | 21256.564 | 20813.464 | 20827.788 | 20944.440 | 20958.422 | 20972.723 |
| 42 | 21227.193 | 21241.535 | 21256.160 | 20812.816 | 20827.479 | 20943.379 | 20957.709 | 20972.365 |
| 43 | 21226.121 | 21240.771 | 21255.755 | 20812.119 | 20827.164 | 20942.330 | 20956.974 | 20971.963 |
| 44 | 21225.004 | 21240.001 | 21255.319 | 20811.457 | 20826.799 | 20941.219 | 20956.226 | 20971.550 |
| 45 | 21223.880 | 21239.205 | 21254.876 | 20810.752 | 20826.405 | 20940.155 | 20955.464 | |
| 46 | 21222.750 | 21238.396 | 21254.394 | 20810.035 | 20826.051 | 20938.968 | 20954.681 | 20970.693 |
| 47 | 21221.575 | 21237.580 | 21253.906 | 20809.298 | 20825.640 | 20937.877 | | 20970.223 |
| 48 | 21220.394 | 21236.726 | 21253.386 | 20808.567 | 20825.274 | 20936.724 | 20953.073 | 20969.768 |
| 49 | 21219.213 | 21235.886 | 21252.879 | 20807.767 | 20824.810 | 20935.552 | 20952.234 | 20969.248 |
| 50 | 21217.968 | 21234.974 | 21252.333 | 20807.009 | 20824.340 | 20934.319 | 20951.383 | 20968.731 |
| 51 | 21216.736 | 21234.094 | | 20806.216 | 20823.903 | 20933.152 | 20950.530 | 20968.208 |
| 52 | 21215.497 | 21233.183 | 21251.216 | 20805.401 | 20823.433 | 20931.962 | 20949.628 | 20967.664 |
| 53 | 21214.251 | 21232.252 | 21250.632 | 20804.550 | 20822.933 | | 20948.730 | |
| 54 | 21212.931 | 21231.302 | 21249.997 | 20803.717 | 20822.433 | 20929.441 | 20947.811 | 20966.518 |
| 55 | 21211.643 | 21230.345 | 21249.367 | 20802.860 | 20821.909 | 20928.171 | 20946.880 | 20965.912 |
| 56 | 21210.309 | 21229.350 | 21248.713 | 20801.987 | 20821.365 | 20926.867 | 20945.926 | 20965.300 |
| 57 | 21208.995 | 21228.349 | 21248.071 | 20801.086 | 20820.798 | 20925.570 | 20944.951 | 20964.624 |
| 58 | 21207.621 | 21227.334 | 21247.384 | 20800.179 | 20820.226 | 20924.241 | 20943.964 | 20963.975 |
| 59 | 21206.254 | 21226.294 | 21246.684 | 20799.260 | 20819.667 | 20922.896 | 20942.962 | 20963.341 |
| 60 | 21204.853 | 21225.235 | 21245.958 | 20798.321 | 20819.024 | 20921.534 | 20941.940 | 20962.641 |
| 61 | 21203.453 | 21224.169 | 21245.214 | 20797.381 | 20818.421 | 20920.165 | 20940.906 | 20961.941 |
| 62 | 21202.032 | 21223.078 | 21244.469 | 20796.390 | 20817.788 | 20918.786 | 20939.848 | 20961.229 |
| 63 | 21200.579 | 21221.961 | 21243.692 | 20795.409 | 20817.140 | 20917.378 | 20938.769 | 20960.466 |
| 64 | 21199.105 | 21220.837 | 21242.935 | 20794.395 | 20816.462 | 20915.924 | 20937.676 | 20959.766 |
| 65 | 21197.632 | 21219.701 | 21242.094 | 20793.409 | 20815.780 | 20914.500 | 20936.580 | 20958.977 |
| 66 | 21196.125 | 21218.526 | 21241.272 | 20792.345 | 20815.071 | 20913.020 | 20935.448 | 20958.182 |
| 67 | 21194.629 | 21217.352 | 21240.424 | 20791.316 | 20814.364 | 20911.566 | 20934.319 | 20957.376 |
| 68 | 21193.078 | 21216.158 | 21239.551 | 20790.221 | 20813.636 | 20910.059 | 20933.152 | 20956.554 |
| 69 | 21191.538 | 21214.938 | 21238.666 | 20789.145 | 20812.866 | | 20931.962 | 20955.718 |
| 70 | 21189.997 | 21213.706 | 21237.775 | 20788.034 | 20812.119 | 20907.042 | | 20954.846 |
| 71 | 21188.462 | 21212.454 | 21236.868 | 20786.929 | 20811.338 | 20905.494 | 20929.556 | |
| 72 | 21186.787 | 21211.189 | 21235.886 | 20785.820 | 20810.534 | 20903.925 | 20928.342 | 20953.073 |
| 73 | 21185.187 | 21209.902 | 21234.974 | 20784.653 | 20809.725 | 20902.356 | 20927.095 | 20952.172 |
| 74 | 21183.541 | 21208.602 | 21233.991 | 20783.490 | 20808.872 | 20900.775 | 20925.827 | 20951.230 |
| 75 | 21181.868 | 21207.279 | 21233.009 | 20782.315 | 20808.049 | 20899.140 | 20924.545 | 20950.269 |
| 76 | 21180.182 | 21205.938 | 21231.995 | 20781.120 | 20807.189 | 20897.507 | 20923.251 | 20949.321 |

Table 1a (*continued*)

| | $[21.3]^3\Delta_3$ (or $^3\Phi_4$)–$X^3\Phi_4$[a] | | | | | $[21.0]^3\Delta_2$ (or $^3\Phi_3$)–$X^3\Phi_3$ | | |
|---|---|---|---|---|---|---|---|---|
| $v'$–$v''$ | 0–0 | | | 0–1 | | 0–0 | | |
| $J''$ | $P$ | $Q$ | $R$ | $Q$ | $R$ | $P$ | $Q$ | $R$ |
| 77 | 21178.530 | 21204.576 | 21230.968 | 20779.914 | 20806.314 | 20895.855 | 20921.933 | 20948.331 |
| 78 | 21176.794 | 21203.190 | | 20778.695 | 20805.401 | 20894.203 | 20920.600 | 20947.335 |
| 79 | 21175.073 | 21201.789 | 21228.869 | 20777.457 | 20804.510 | | 20919.250 | 20946.311 |
| 80 | 21173.338 | 21200.391 | 21227.790 | 20776.196 | 20803.597 | 20890.820 | 20917.886 | 20945.282 |
| 81 | 21171.562 | 21198.965 | 21226.667 | 20774.910 | 20802.647 | 20889.098 | 20916.497 | 20944.240 |
| 82 | 21169.813 | 21197.515 | 21225.582 | | 20801.666 | 20887.381 | 20915.103 | 20943.148 |
| 83 | 21168.004 | 21196.064 | 21224.439 | | 20800.711 | 20885.626 | 20913.687 | 20942.079 |
| 84 | 21166.169 | 21194.574 | 21223.277 | | 20799.721 | 20883.858 | 20912.248 | |
| 85 | 21164.354 | 21193.078 | 21222.121 | | 20798.720 | 20882.059 | 20910.789 | 20939.860 |
| 86 | 21162.506 | 21191.538 | 21220.916 | | 20797.668 | 20880.279 | 20909.317 | |
| 87 | 21160.658 | 21189.997 | 21219.701 | | 20796.686 | 20878.411 | 20907.834 | 20937.543 |
| 88 | 21158.758 | 21188.462 | 21218.480 | | 20795.570 | 20876.602 | 20906.330 | 20936.352 |
| 89 | | 21186.864 | 21217.249 | | 20794.532 | 20874.743 | 20904.808 | 20935.182 |
| 90 | 21154.917 | 21185.291 | 21215.985 | | 20793.409 | 20872.896 | | 20933.965 |
| 91 | 21152.989 | 21183.673 | 21214.701 | | 20792.345 | 20870.996 | 20901.706 | 20932.715 |
| 92 | 21151.029 | 21182.049 | 21213.395 | | | 20869.123 | 20900.122 | 20931.481 |
| 93 | 21149.055 | 21180.405 | 21212.081 | | | 20867.196 | 20898.535 | 20930.207 |
| 94 | 21147.056 | 21178.736 | 21210.754 | | | | 20896.922 | 20928.903 |
| 95 | | 21177.061 | 21209.380 | | | | 20895.323 | 20927.656 |
| 96 | 21143.016 | 21175.353 | 21207.999 | | | | 20893.660 | 20926.287 |
| 97 | 21140.977 | 21173.652 | 21206.652 | | | | 20892.014 | 20925.018 |
| 98 | | 21171.905 | 21205.205 | | | | 20890.309 | 20923.641 |
| 99 | | 21170.153 | 21203.778 | | | | 20888.613 | |
| 100 | | 21168.374 | 21202.338 | | | | 20886.917 | 20920.865 |
| 101 | | 21166.583 | 21200.884 | | | | 20885.183 | 20919.460 |
| 102 | | 21164.773 | 21199.397 | | | | 20883.439 | |
| 103 | | 21162.950 | 21197.877 | | | | 20881.675 | 20916.586 |
| 104 | | 21161.094 | 21196.364 | | | | 20879.867 | 20915.100 |
| 105 | | 21159.240 | 21194.818 | | | | 20878.088 | |
| 106 | | 21157.346 | 21193.265 | | | | 20876.230 | |
| 107 | | 21155.459 | 21191.691 | | | | 20874.409 | |
| 108 | | 21153.552 | 21190.085 | | | | 20872.548 | |
| 109 | | 21151.607 | 21188.466 | | | | 20870.681 | |
| 110 | | 21149.648 | 21186.860 | | | | 20868.779 | |
| 111 | | 21147.658 | 21185.187 | | | | 20866.885 | |
| 112 | | | 21183.541 | | | | 20864.936 | |
| 113 | | 21143.665 | 21181.868 | | | | | |
| 114 | | 21141.634 | 21180.143 | | | | | |
| 115 | | 21139.603 | 21178.424 | | | | | |
| 116 | | 21137.546 | | | | | | |
| 117 | | 21135.448 | | | | | | |
| 118 | | 21133.324 | | | | | | |
| 119 | | 21131.247 | | | | | | |
| 120 | | 21129.083 | | | | | | |
| 121 | | 21126.966 | | | | | | |
| 122 | | 21124.769 | | | | | | |
| 123 | | 21122.552 | | | | | | |
| 124 | | 21120.342 | | | | | | |
| 125 | | 21118.125 | | | | | | |

[a] This transition was previously attributed to $[21.0]^3\Phi_4$–$X^3\Phi_4$ by Adam et al. [10]. For further details, see text.

the ground state. No other spin components were seen in either the low or the high resolution experiments because the molecules were cooled in the jet expansion.

In this paper, we present our Fourier transform emission spectra that show the bands previously obtained by Adam et al. [10] and also new bands involving the $\Omega = 3$ spin component of the ground state. An improved and extended set of molecular constants is also provided.

## 2. Experimental details

The experimental details were described earlier [18]. A stable DC discharge was generated in a high temperature tube furnace. Commercially available $CoCl_2$ powder was placed near the center in a 1.2 m long, 5 cm diameter alumina tube, and heated up to 550 °C by the furnace. The pressure was kept around 5 Torr by a slow

Table 1b

| | $[20.7]^3\Phi_4$–$X^3\Phi_4$ | | | | | |
|---|---|---|---|---|---|---|
| $v'$–$v''$ | 0–0 | | 1–0 | | 0–1 | |
| $J''$ | $P$ | $R$ | $P$ | $R$ | $P$ | $R$ |
| 10 | 20675.976 | | | | | |
| 11 | 20675.395 | | | | | |
| 12 | 20674.804 | | | | | |
| 13 | 20674.199 | | | | | |
| 14 | 20673.555 | | | | | |
| 15 | 20672.909 | | | | | |
| 16 | 20672.187 | | 21073.016 | | | |
| 17 | 20671.498 | | 21072.261 | | | |
| 18 | 20670.775 | | 21071.519 | | | |
| 19 | | | 21070.725 | 21083.849 | | |
| 20 | 20669.284 | 20683.140 | 21069.951 | 21083.682 | | |
| 21 | 20668.499 | 20683.016 | 21069.114 | 21083.553 | 20238.503 | |
| 22 | 20667.691 | 20682.874 | 21068.266 | 21083.339 | 20237.733 | |
| 23 | 20666.867 | 20682.710 | 21067.379 | 21083.143 | 20236.962 | |
| 24 | 20666.019 | 20682.530 | 21066.481 | 21082.913 | 20236.131 | 20252.689 |
| 25 | 20665.144 | 20682.338 | 21065.561 | 21082.671 | 20235.322 | 20252.515 |
| 26 | | 20682.112 | 21064.623 | 21082.414 | 20234.462 | 20252.351 |
| 27 | 20663.336 | 20681.869 | 21063.658 | 21082.099 | 20233.598 | 20252.158 |
| 28 | 20662.387 | 20681.603 | 21062.669 | 21081.773 | 20232.723 | |
| 29 | 20661.421 | 20681.315 | 21061.665 | | | 20251.712 |
| 30 | 20660.438 | 20681.004 | 21060.615 | 21081.056 | 20230.890 | 20251.458 |
| 31 | 20659.444 | 20680.677 | 21059.543 | 21080.667 | 20229.961 | 20251.190 |
| 32 | 20658.416 | 20680.321 | 21058.470 | 21080.252 | 20228.982 | 20250.889 |
| 33 | 20657.371 | 20679.954 | 21057.370 | 21079.820 | 20228.002 | 20250.589 |
| 34 | 20656.292 | 20679.558 | 21056.242 | 21079.359 | | 20250.250 |
| 35 | 20655.213 | 20679.146 | 21055.080 | 21078.882 | 20225.978 | 20249.903 |
| 36 | | 20678.705 | 21053.906 | 21078.371 | 20224.942 | 20249.532 |
| 37 | 20652.971 | 20678.242 | 21052.704 | 21077.838 | 20223.879 | 20249.142 |
| 38 | 20651.818 | 20677.756 | 21051.491 | 21077.282 | 20222.809 | 20248.737 |
| 39 | 20650.643 | 20677.248 | 21050.232 | 21076.693 | 20221.702 | 20248.310 |
| 40 | 20649.451 | 20676.728 | | 21076.109 | 20220.584 | 20247.863 |
| 41 | 20648.237 | 20676.180 | | 21075.475 | 20219.450 | 20247.394 |
| 42 | 20647.005 | 20675.616 | 21046.368 | 21074.824 | 20218.290 | 20246.914 |
| 43 | 20645.740 | 20675.028 | 21045.043 | 21074.167 | 20217.119 | 20246.407 |
| 44 | 20644.452 | 20674.412 | 21043.678 | 21073.465 | 20215.922 | 20245.876 |
| 45 | 20643.159 | 20673.780 | 21042.294 | 21072.752 | 20214.699 | 20245.331 |
| 46 | 20641.837 | 20673.124 | 21040.890 | 21072.016 | 20213.468 | 20244.762 |
| 47 | | 20672.447 | 21039.448 | 21071.242 | 20212.220 | 20244.175 |
| 48 | 20639.125 | 20671.752 | 21037.998 | 21070.461 | 20210.944 | 20243.583 |
| 49 | 20637.736 | 20671.040 | 21036.515 | 21069.642 | 20209.646 | 20242.958 |
| 50 | 20636.329 | 20670.289 | 21035.020 | 21068.811 | 20208.348 | 20242.309 |
| 51 | 20634.911 | 20669.533 | 21033.506 | 21067.952 | 20207.001 | 20241.642 |
| 52 | 20633.448 | 20668.753 | 21031.963 | 21067.071 | 20205.665 | 20240.961 |
| 53 | 20631.974 | 20667.951 | 21030.395 | 21066.178 | 20204.293 | 20240.251 |
| 54 | 20630.483 | 20667.127 | 21028.800 | 21065.263 | 20202.905 | 20239.551 |
| 55 | 20628.969 | 20666.273 | | 21064.314 | 20201.487 | 20238.795 |
| 56 | 20627.432 | 20665.404 | 21025.561 | 21063.332 | 20200.073 | 20238.043 |
| 57 | 20625.879 | 20664.511 | 21023.904 | 21062.334 | 20198.617 | 20237.252 |
| 58 | 20624.297 | 20663.602 | 21022.228 | 21061.322 | 20197.147 | 20236.450 |
| 59 | 20622.704 | 20662.670 | 21020.536 | 21060.295 | 20195.666 | 20235.632 |
| 60 | 20621.083 | 20661.716 | 21018.817 | 21059.228 | 20194.162 | 20234.796 |
| 61 | 20619.439 | 20660.743 | | 21058.156 | 20192.639 | 20233.937 |
| 62 | 20617.784 | 20659.743 | 21015.294 | 21057.050 | 20191.094 | 20233.056 |
| 63 | 20616.095 | 20658.727 | 21013.510 | 21055.927 | 20189.534 | 20232.158 |
| 64 | 20614.395 | 20657.687 | 21011.706 | 21054.788 | 20187.952 | 20231.246 |
| 65 | 20612.672 | 20656.620 | 21009.882 | 21053.643 | 20186.362 | |
| 66 | 20610.919 | 20655.535 | 21008.026 | 21052.475 | 20184.742 | 20229.352 |
| 67 | 20609.158 | | | 21051.242 | | 20228.380 |
| 68 | 20607.368 | 20653.309 | | | 20181.439 | 20227.381 |
| 69 | 20605.567 | 20652.174 | | | 20179.774 | 20226.371 |
| 70 | 20603.742 | 20651.016 | | | 20178.087 | 20225.342 |

Table 1b (*continued*)

| | $[20.7]^3\Phi_4$–$X^3\Phi_4$ | | | | | |
|---|---|---|---|---|---|---|
| $v'$–$v''$ | 0–0 | | 1–0 | | 0–1 | |
| $J''$ | $P$ | $R$ | $P$ | $R$ | $P$ | $R$ |
| 71 | 20601.895 | 20649.824 | | | 20176.362 | 20224.306 |
| 72 | 20600.025 | 20648.615 | | | 20174.645 | |
| 73 | 20598.144 | 20647.395 | | | 20172.891 | |
| 74 | 20596.235 | | | | 20171.140 | |
| 75 | 20594.314 | | | | 20169.352 | |
| 76 | 20592.383 | | | | 20167.571 | |
| 77 | 20165.779 | | | | | |

Table 1c

| | $[20.4]^3\Phi_3$–$X^3\Phi_3$ | | | |
|---|---|---|---|---|
| $v'$–$v''$ | 0–0 | | 0–1 | |
| $J''$ | $P$ | $R$ | $P$ | $R$ |
| 13 | 20369.011 | | | |
| 14 | 20368.389 | | | |
| 15 | 20367.738 | | 19940.567 | |
| 16 | 20367.045 | | 19939.905 | |
| 17 | 20366.342 | | 19939.242 | |
| 18 | 20365.640 | | 19938.544 | |
| 19 | 20364.889 | | 19937.846 | |
| 20 | 20364.122 | 20377.931 | 19937.123 | |
| 21 | 20363.341 | 20377.822 | 19936.377 | 19950.885 |
| 22 | 20362.525 | 20377.696 | 19935.599 | 19950.783 |
| 23 | 20361.705 | 20377.545 | 19934.850 | 19950.688 |
| 24 | 20360.848 | 20377.364 | 19934.036 | 19950.556 |
| 25 | 20359.982 | 20377.166 | 19933.225 | 19950.389 |
| 26 | 20359.082 | 20376.939 | 19932.376 | 19950.226 |
| 27 | 20358.174 | 20376.704 | 19931.495 | 19950.036 |
| 28 | 20357.245 | 20376.439 | 19930.644 | 19949.825 |
| 29 | 20356.287 | 20376.157 | 19929.724 | 19949.609 |
| 30 | 20355.303 | 20375.855 | 19928.821 | 19949.377 |
| 31 | 20354.303 | 20375.523 | 19927.878 | 19949.092 |
| 32 | 20353.290 | 20375.178 | 19926.924 | 19948.818 |
| 33 | 20352.247 | 20374.812 | 19925.944 | 19948.505 |
| 34 | | 20374.400 | 19924.954 | 19948.185 |
| 35 | 20350.087 | 20374.001 | 19923.950 | 19947.838 |
| 36 | 20348.994 | 20373.572 | 19922.915 | 19947.471 |
| 37 | 20347.868 | | 19921.853 | 19947.105 |
| 38 | 20346.728 | | 19920.783 | 19946.691 |
| 39 | 20345.560 | 20372.143 | 19919.684 | 19946.275 |
| 40 | 20344.379 | 20371.630 | 19918.592 | |
| 41 | 20343.164 | 20371.088 | 19917.456 | |
| 42 | 20341.937 | 20370.520 | 19916.315 | 19944.907 |
| 43 | 20340.676 | 20369.932 | 19915.155 | 19944.403 |
| 44 | 20339.406 | 20369.343 | 19913.959 | 19943.889 |
| 45 | 20338.112 | 20368.709 | 19912.754 | 19943.359 |
| 46 | 20336.796 | 20368.061 | 19911.523 | 19942.814 |
| 47 | 20335.451 | | 19910.306 | 19942.227 |
| 48 | 20334.102 | 20366.754 | 19909.023 | 19941.678 |
| 49 | 20332.731 | 20365.972 | 19907.743 | 19940.983 |
| 50 | 20331.373 | 20365.249 | | 19940.364 |
| 51 | 20329.869 | 20364.497 | | 19939.706 |
| 52 | 20328.452 | 20363.706 | | 19939.047 |
| 53 | 20326.985 | 20362.924 | | 19938.359 |
| 54 | 20325.501 | 20362.113 | | 19937.646 |
| 55 | 20323.996 | 20361.268 | | 19936.902 |

Table 1c (*continued*)

| | $[20.4]^3\Phi_3$–$X^3\Phi_3$ | | | |
|---|---|---|---|---|
| $v'$–$v''$ | 0–0 | | 0–1 | |
| $J''$ | $P$ | $R$ | $P$ | $R$ |
| 56 | 20322.458 | 20360.402 | | 19936.156 |
| 57 | 20320.923 | 20359.524 | | 19935.401 |
| 58 | 20319.360 | 20358.616 | | 19934.615 |
| 59 | 20317.762 | 20357.708 | | 19933.811 |
| 60 | | 20356.749 | | 19932.996 |
| 61 | 20314.521 | 20355.770 | | 19932.149 |
| 62 | 20312.874 | 20354.803 | | 19931.270 |
| 63 | 20311.201 | 20353.777 | | 19930.380 |
| 64 | 20309.502 | 20352.747 | | 19929.473 |
| 65 | 20307.787 | 20351.688 | | 19928.541 |
| 66 | 20306.064 | 20350.642 | | 19927.621 |
| 67 | 20304.294 | 20349.523 | | 19926.637 |
| 68 | 20302.524 | 20348.414 | | 19925.678 |
| 69 | 20300.717 | 20347.270 | | 19924.679 |
| 70 | | 20346.115 | | 19923.667 |
| 71 | 20297.060 | 20344.917 | | 19922.649 |
| 72 | 20295.206 | 20343.745 | | 19921.583 |
| 73 | 20293.327 | 20342.509 | | 19920.503 |
| 74 | 20291.427 | 20341.273 | | 19919.416 |
| 75 | 20289.506 | 20340.003 | | |
| 76 | 20287.568 | 20338.742 | | |
| 77 | | 20337.410 | | |
| 78 | | 20336.111 | | |
| 79 | | 20334.740 | | |
| 80 | | 20333.370 | | |
| 81 | | 20331.996 | | |
| 82 | | 20330.575 | | |
| 83 | | 20329.148 | | |
| 84 | | 20327.681 | | |
| 85 | | 20326.229 | | |
| 86 | | 20324.707 | | |
| 87 | | 20323.195 | | |

flow of Ar buffer gas. The ends of the cell were sealed with $CaF_2$ windows. Two stainless steel sheets were rolled into cylindrical electrodes and placed inside the ends of the ceramic tube. A ~3 kV, 300 mA DC discharge were operated between these electrodes. The light emission was collected by a $CaF_2$ lens and sent into the entrance aperture of the spectrometer.

The spectrometer used was a Bruker IFS 120 HR Fourier transform spectrometer at the University of Waterloo. The spectrometer was equipped with a visible quartz beamsplitter and was not evacuated during the measurement. A photomultiplier tube was placed at the "back parallel exit" to reduce the number of mirror reflections and to increase the sensitivity of the spectrometer. Just before the photomultiplier tube, 450 nm red pass and 550 nm blue pass filters were inserted to minimize the influence of strong atomic lines and the internal He–Ne laser radiation. In total 130 scans were accumulated at a spectral resolution of 0.05 $cm^{-1}$. Because the spectrometer was not evacuated, the spectral lines were converted to vacuum wavenumbers as described previously [19]. The calibration factor was obtained as 1.000001167 on the basis of standard Ar atomic lines [20]. The observed line positions were listed in Table 1a–1c.

## 3. Description of the observed bands

The observed spectra are shown in Fig. 1. As shown in Fig. 1, there are numerous bandheads seen near 480 nm. Considering the spectra previously reported by Adam et al. [10], one can easily identify some bands denoted as $A(1)$ and $B(1)$ in the figure, but our spectra appear different from the high resolution laser excitation spectra. In the previous work, Adam et al. [10] employed the molecular beam method so transitions that do not connect to the ground state are relatively weak, and thus harder to observe. However, in our work the molecules were excited not only in a DC discharge but also by heating in the tube furnace. This allowed us to obtain easily bands involving vibrationally excited states as well as other spin components. We have also seen new emission bands in the 1 μm region and these new tran-

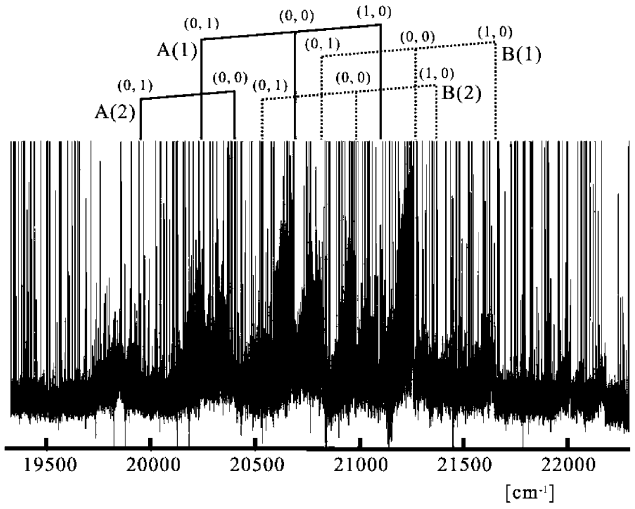


Fig. 1. Overview spectra of CoCl in the 500 nm region.

sitions have even more highly excited vibrational levels than in the bands reported here. The analysis of our 1 μm data is still in progress.

1. The $[20.7]^3\Phi_4$–$X^3\Phi_4$ transition. The intense band, denoted as $A(1)$ in Fig. 1, was studied by Adam et al. [10], who assigned it as the $[20.7]^3\Phi_4$–$X^3\Phi_4$ transition. The 0–0 band (the bandhead is located at 20683.6 $cm^{-1}$), 1–0 (head at 21084.1 $cm^{-1}$), and 0–1 (head at 20253.2 $cm^{-1}$) bands of this transition have been rotationally analyzed. These bands consist of $P$ and $R$ branches up to $J \sim 80$, but no $Q$ branch is seen. As seen in Fig. 2, all hyperfine components are blended into one rotational line, but the extrapolated line positions for low-$J$ values agree quite well with those deduced from the constants of [10] after removing the hyperfine interaction term. Although a $Q$ branch has been observed at low-$J$ in the previous high resolution study [10], the absence of a $Q$ branch in our spectra is consistent with the assignment as a $\Delta\Omega = 0$ transition.

2. The [21.3]-$X^3\Phi_4$ transition. The band denoted as $B(1)$ in Fig. 1 was labeled $[21.3]^3\Phi_4$–$X^3\Phi_4$ by Adam et al. [10]. They cite two pieces of evidence for this assignment. Firstly, their low resolution spectra suggest that the intensities of the $P$ and $R$ branches are similar, indicating a $\Delta\Lambda = 0$ transition. This feature is consistent with the result of Suresh Kumar and Srikant [9], who claimed the band around 470 nm region exhibits no $Q$ branch. Secondly, CoCl is similar to CoF and CoH, which both have two close-lying excited $^3\Phi$ states arising from the same electronic configuration. The excited state rotational and hyperfine constants support this interpretation [21].

In our study, the 0–0 and 0–1 bands of the $B(1)$ band exhibit intense $Q$ branches, as illustrated in Fig. 3. In the case of the 0–0 band, for example, the $Q$ branch is observed from $J = 17$ to $J = 112$. At first sight, the presence of a well-developed $Q$ branch suggests that the studied transition has $\Delta\Omega \neq 0$. This conclusion, however, is in contradiction with the interpretation given by Adam et al. [10]. Unfortunately, our experimental line positions do not overlap with those given by Adam et al. [10], and no hyperfine structure has been seen in our spectra. In addition, discrepancies up to 0.2 $cm^{-1}$ are seen between extrapolated wavenumbers of lines calculated with our constants and those deduced from [10], after removing the hyperfine interaction term.

3. The $[20.4]^3\Phi_3$–$X^3\Phi_3$ transition. As already mentioned, several bands such as those denoted as $A(2)$ and $B(2)$ in Fig. 1 are observed to be stronger in our spectra than in Fig. 1 of [10]. One can expect that these bands are associated with other spin–orbit components of the two already identified transitions. A tentative confirmation can be obtained by comparing the vibrational interval, $\Delta G_{1/2}$, of the states involved in the transitions with those of the states marked as $A(1)$ and $B(1)$. For the $A(2)$ band, it is easy to identify a set of two bands at 20 378 and 19 951 $cm^{-1}$. These two bands are separated by 427 $cm^{-1}$, which is close to 430 $cm^{-1}$, observed for the $X^3\Phi_4$ ground state. The absence of any $Q$ branch, and the similarity of the vibrational and rotational constants (as listed in Table 2) are convincing evidence that these two bands should be identified as 0–0 and 0–1 bands of the $[20.4]^3\Phi_3$–$X^3\Phi_3$ transition. Note that a trace of a bandhead-like feature is observed at 20 795 $cm^{-1}$, near where the 1–0 band is expected to lie.

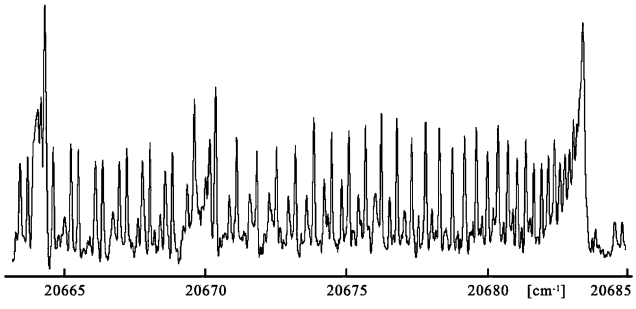


Fig. 2. A portion of the spectra of the $[20.7]^3\Phi_4$–$X^3\Phi_4$ 0–0 band.

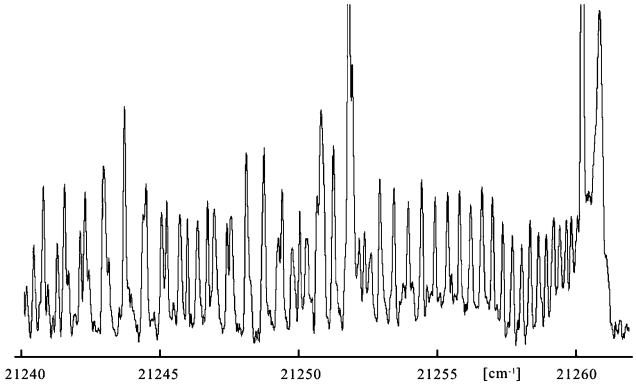


Fig. 3. A portion of the spectra of the [21.3]-$X^3\Phi_4$ 0–0 band.

Table 2
Effective molecular constants for $Co^{35}Cl$[a]

| $v$ | $T$ | $B$ | $D \times 10^7$ | $T$ | $B$ | $D \times 10^7$ |
|---|---|---|---|---|---|---|
| | $X^3\Phi_i\ \Omega = 3$ | | | $X^3\Phi_i\ \Omega = 2$ | | |
| 0 | 0 | 0.1796368(16) | 1.2986(41) | $E$[b] | 0.1793100(17) | 1.2788(58) |
| | | [0.1797378(83)][c] | [1.3(fixed)] | | | |
| 1 | 430.418(5) | 0.1786897(30) | 1.3178(70) | $E + 427.412(5)$ | 0.1783199(44) | 1.294(10) |
| | $[20.4]^3\Phi_i\ \Omega = 4$ | | | $[20.4]^3\Phi_i\ \Omega = 3$ | | |
| 0 | 20680.568(4) | 0.1688653(13) | 1.2257(46) | $E + 20375.358(5)$ | 0.1686094(14) | 1.2083(56) |
| | [20680.5649(4)] | [0.1689708(93)] | [1.2(fixed)] | | | |
| 1 | 21081.590(5) | 0.1678720(43) | 1.0437(93) | | | |
| | [21081.5447(6)] | [0.168053(11)] | [1.22(17)] | | | |
| | $[21.0]F_1$[d] | | | $[21.0]F_2$ | | |
| 0 | 21257.351(4) | 0.1708816(11) | 1.3519(42) | $E + 20973.022(5)$ | 0.1708341(12) | 1.3288(58) |
| | [21257.2495(6)] | [0.1714058(36)] | [l.3(fixed)] | | | |

[a] In $cm^{-1}$ units. All numbers in parentheses denote one standard deviation for the last significant figure.
[b] The undetermined energy level difference between the $v = 0$ levels of $X^3\Phi$, $\Omega = 4$ and $\Omega = 3$.
[c] The numbers in square brackets are the values from [10].
[d] This state was previously assigned as $^3\Phi_i$, in [10]. See text for more details.

Overlapping, however, by the 0–1 band of the [21.3] $X^3\Phi_4$ transition prevents us from confirming this assignment by rotational analysis.

4. The [21.0]-$X^3\Phi_3$ transition. The band labeled as $B(2)$ in Fig. 1 has $P$, $Q$, and $R$ branches. One member of the progression is intense and is located at 20 977 $cm^{-1}$, and two weak features appear at 20 550 and 21 367 $cm^{-1}$. The spacing between the bandheads at 20 977 and 20 550 $cm^{-1}$ is identical to the $\Delta G''_{1/2}$ value of 427.4 $cm^{-1}$ for the $X^3\Phi_3$ state. In addition, the spacing between the two heads at 20 977 and 21 367 $cm^{-1}$ is close to the $\Delta G'_{1/2}$ value of 391 $cm^{-1}$ of the $[21.3]^3\Phi_4$ state in [10]. Following a rotational analysis, the rotational constants for the lower levels of these three bands are found to agree well with those of the newly identified $X^3\Phi_3$ state, and the rotational constants for upper state are found to be similar to those of the upper state of the $A(1)$ band. This suggests that these bands should be the 0–0 (20 977 $cm^{-1}$), the 0–1 (20 550 $cm^{-1}$), and the 1–0 (21 367 $cm^{-1}$) bands of the [21.0]-$X^3\Phi_3$ transition.

Note that several weak bandhead features were also seen in our spectra. These features will be identified by dispersed laser-induced fluorescence experiments which are in progress.

## 4. Analysis and discussion

In the first stage of our analysis we assumed that the energy levels of CoCl can be represented by the usual $J(J+1)$ polynomial formula in order to determine effective molecular constants. After identifying all rotationally resolved bands involving the $X^3\Phi_4$ state (with bandheads located at 21 261, 20 832, 20 253, 20 683, and 21 084 $cm^{-1}$), these bands have been fitted simultaneously. Similarly the bands at 19 951, 20 378, and 20 977 $cm^{-1}$ that connect with the $X^3\Phi_3$ state were fitted simultaneously. The constants thus determined are listed in Table 2. The effective rotational constants for both $X^3\Phi_4$ and $[20.4]^3\Phi_4$ states agree well with the previous values reported in [10]. On the other hand, our rotational constants for the [21.3] state are not in very good agreement with the previous values [10]. In the previous section we mentioned that the discrepancies between the extrapolated line positions and the hyperfine-free positions for the low-$J$ transitions are up to 0.2 $cm^{-1}$. However, this is not completely unacceptable because our extrapolated line positions do lie within the hyperfine components corresponding to the appropriate $J$ as reported in [10]. Moreover, in their analysis, Adam

Table 3
Molecular constants for $Co^{35}Cl$ from a Hund's case ($a$) analysis[a]

| | $X^3\Phi_i\ v = 0$ | $X^3\Phi_i\ v = 1$ | $[20.4]^3\Phi_i\ v = 0$ | $[21.0]^3\Delta_i\ v = 0$ |
|---|---|---|---|---|
| $T$ | 0.0 | 427.4100(34) | 20375.3781(22) | 20973.0327(15) |
| $A_{SO}$ | −233[b] | −231.9964(13) | −131.29410(81) | −207.53243(90)[c] |
| $A_D \times 10^4$ | 1.091(23) | 1.212(24) | 1.037(23) | 0.449(35)[c] |
| $B$ | 0.1793172(79) | 0.1783308(84) | 0.1686174(79) | 0.1708456(79) |
| $D \times 10^7$ | 1.2618(58) | 1.2831(71) | 1.1928(59) | 1.3159(58) |

[a] In $cm^{-1}$ units. All numbers in parentheses are one standard deviation for the last significant figure.
[b] The spin–orbit interaction parameter for $X^3\Phi_i\ v = 0$ is constrained to that of CoF in the $X^3\Phi_i\ v = 0$ state, taken from [17].
[c] These constants were also determined by using a Hamiltonian for $^3\Phi_i$, state for the [21.0] state. In this case, the values are $A_{SO} = -138.24137(61)$ and $A_D = 2.98(23) \times 10^{-5} cm^{-1}$. The term values and rotational constants remained the same for either $^3\Phi_i$ or $^3\Delta_i$. For further details, see the text.

et al. [10] fixed the centrifugal distortion constants, causing a small shift in the rotational constant. Because Adam et al. saw the $R(4)$, $Q(4)$, and $P(5)$ lines, the quantum number $\Omega$ in the upper electronic state could be 4 or 3 and the most likely electronic states are either $^3\Phi_4$ or $^3\Delta_3$. Evidently Adam et al. [10] favor the $^3\Phi_4$ assignment while our data are more consistent with a $^3\Delta_3$ assignment for the [21.3] state.

The electronic structure of an ionic molecule ($M^{\delta+}X^{\delta-}$) correlates with that of the atomic metal ion ($M^+$) as well as with isovalent molecules [22]. The spin–orbit constant for the ground state of CoF, $A_{SO}(X^3\Phi_i)$ is about $-233\,cm^{-1}$ [17], and we can use this value for a Hund's case ($a$) fit of the 0–0 and 0–1 bands of $[20.7]^3\Phi_4$–$X^3\Phi_4$ and $[20.4]^3\Phi_3$–$X^3\Phi_3$, transitions and 0–0 bands of [21.3]-$X^3\Phi_4$ and [21.0]-$X^3\Phi_3$ transitions of CoCl. In this step, Brown's $\mathbf{N}^2$ reduced Hamiltonian [23] was employed, and the spin–orbit interaction constant for the ground state ($v = 0$) was constrained to $-233\,cm^{-1}$, and the spin–spin interaction parameter $\lambda$ was assumed to be negligible. The molecular constants are listed in Table 3. In this process, we assumed that the [21.0] and [21.3] states should be $F_2$ and $F_1$ components of either a $^3\Delta_i$ or a $^3\Phi_i$ state, respectively. The spin–orbit interaction parameter for the $X^3\Phi_i$, $v = 1$ state ($-231\,cm^{-1}$) shows a slight change from that for $v = 0$. On the other hand, the spin–orbit constants for the excited states appear to be very different from that of CoF in the $[18.8]^3\Phi_i$ state, which correlates with $[20.4]^3\Phi_i$ state of CoCl. The spin–orbit constants for the $[20.4]^3\Phi_i$ and [21.0] states are obtained as $-131.29410(81)\,cm^{-1}$, and $-207.53243(90)\,cm^{-1}$ (in case of a $[21.0]^3\Delta_i$ state) or $-138.24137(61)\,cm^{-1}$ (in case of a $[21.0]^3\Phi_i$ state), respectively, while $A_{SO}$ is about $-196\,cm^{-1}$ for the $[18.8]^3\Phi$ state of CoF [16].

We assume that these excited states directly correlate with the atomic $b^3P$ state ((core)$3d^7(a^4P)4s$) of $Co^+$, which is located at $24\,200\,cm^{-1}$ above the atomic ground state, $a^3F$ ((core)$3d^8$). The atomic spin–orbit parameter, $\zeta$, for the $b^3P$ state is $-120.2\,cm^{-1}$, derived from the atomic energy levels reported by Moore [24]. It is also assumed that the electronic configurations of these excited states can be represented by

$$(\text{core})(10\sigma)^2(4\pi)^4(1\delta)^3(5\pi)^3(11\sigma)^1(12\sigma)^1 \quad [20.4]^3\Phi_i \text{ and } [21.0]^3\Phi_i,$$

$$(\text{core})(10\sigma)^2(4\pi)^4(1\delta)^3(5\pi)^4(11\sigma)^0(12\sigma)^1 \qquad [21.0]^3\Delta_i.$$

With these assumptions, one can easily obtain the relationship $A_{SO} \sim \zeta$, for these three excited states of CoCl. This relationship works well for the $[20.4]^3\Phi_i$ state of CoCl with $A_{SO} = -131.29410(81)\,cm^{-1}$ and $\zeta = -120.2\,cm^{-1}$ for $Co^+$ in $b^3P$ state. If this relationship is also valid for the [21.0] state, then this state is more likely to be $^3\Phi_i$ than $^3\Delta_i$. Unfortunately, such a simple relationship is generally not reliable particularly for excited states, because molecular wavefunctions are composed of mixtures of atomic states. Even the isovalent CoF molecule does not obey this relationship in the $[18.8]^3\Phi_i$ state [17]. Although we favor the $^3\Delta_3$ assignment for the excited state of the [21.3]-$X^3\Phi_4$ transition (and $^3\Delta_2$ for the [21.0]-$X^3\Phi_3$ sub-band), additional experimental and/or theoretical work is needed for confirmation.

In conclusion, we have identified two spin components for the $[20.4]^3\Phi_i$–$X^3\Phi_i$ and [21.0]-$X^3\Phi_i$ transitions. Improved effective molecular constants were obtained and our rotational assignment agrees with the previous work [10]. Identification of a second spin component of these two transitions allows us to perform Hund's case ($a$) fits to obtain effective spin orbit constants for the $[20.4]^3\Phi_i$ and [21.0] states. The [21.0] state is probably $^3\Delta_i$ but we cannot definitely rule out the $^3\Phi_i$ assignment.

## Acknowledgments

The authors are thankful to Profs. A.G. Adam and C. Linton of the University of New Brunswick for providing their line list and for fruitful discussions. This research has been supported by the Natural Sciences and Engineering Research Council (NSERC) of Canada. Centre d'Etudes et de Recherches Lasers et Applications is supported by Ministère Chargé de la Recherche, Région Nord-Pas de Calais and Fond Européen de Développement Economique des Régions.

## References

[1] P. Mesnage, C. R. Acad. Sci. 201 (1935) 389–391.
[2] K.R. More, Phys. Rev. 54 (1938) 122–125.
[3] V.G. Krishnamurty, Ind. J. Phys. 26 (1952) 177–185.
[4] S.V.K. Rao, P.T. Rao, Ind. J. Phys. 35 (1961) 556–561.
[5] D.W. Green, D.P. McDermott, A. Bergman, J. Mol. Spectrosc. 98 (1983) 111–124.
[6] C.V. Reddy, A.L. Narayana, P.T. Rao, Ind. J. Pure Appl. Phys. 22 (1984) 550.
[7] C.V. Reddy, A.L. Narayana, P.T. Rao, Opt. Pure Appl. 17 (1985) 289–296.
[8] A.B. Darji, M.B. Suresh Kumar, N.R. Shah, P.M. Shah, Ind. J. Pure Appl. Phys. 26 (1988) 44–46.
[9] M.B. Suresh Kumar, S.R. Srikant, Turk. J. Phys. 22 (1998) 21.
[10] A.G. Adam, J.R.D. Peers, Y. Teng, C. Linton, J. Mol. Spectrosc. 212 (2002) 111–117.
[11] M. Freindorf, C.M. Marian, B.A. Hess, J. Chem. Phys. 99 (1993) 1215–1223.
[12] M.A. Barnes, A.J. Merer, G.F. Metha, J. Mol. Spectrosc. 173 (1995) 100–112.
[13] R.S. Ram, P.F. Bernath, S.P. Davis, J. Mol. Spectrosc. 175 (1996) 1–6.
[14] A.G. Adam, L.P. Fraser, W.D. Hamilton, M.C. Steeves, Chem. Phys. Lett. 230 (1994) 82–86.

[15] R.S. Ram, P.F. Bernath, S.P. Davis, J. Mol. Spectrosc. 173 (1995) 158–176.
[16] R.S. Ram, P.F. Bernath, S.P. Davis, J. Chem. Phys. 104 (1996) 6949–6955.
[17] A.G. Adam, W.D. Hamilton, J. Mol. Spectrosc. 206 (2001) 139–142.
[18] Y. Krouti, T. Hirao, C. Dufour, A. Boulezhar, B. Pinchemel, P.F. Bernath, J. Mol. Spectrosc. 214 (2002) 152–174.
[19] T. Hirao, B. Pinchemel, P.F. Bernath, J. Mol. Spectrosc. 202 (2000) 213–222.
[20] G. Norlén, Phys. Scr. 8 (1973) 249–268.
[21] R.A. Frosch, H.M. Foley, Phys. Rev. 88 (1952) 1337–1349.
[22] R.W. Field, Ber. Bunsenges. Phys. Chem. 86 (1982) 771–779; S.F. Rice, H. Martin, R.W. Field, J. Chem. Phys. 82 (1985) 5023–5034.
[23] J.M. Brown, E.A. Colbourn, J.K.G. Watson, F.D. Wayne, J. Mol. Spectrosc. 74 (1979) 294–318.
[24] C.E. Moore, in: Atomic Energy Levels, Vol. II, National Bureau of Standards, Gaithersburg, MD, 1952.